JACS
JOURNAL OF THE AMERICAN CHEMICAL SOCIETY
Communication
pubs.acs.org/JACS

Urease-Mediated Room-Temperature Synthesis of Nanocrystalline Titanium Dioxide

John M. Johnson, Nichola Kinsinger, Chhay Sun, Dongsheng Li,† and David Kisailus*

Department of Chemical and Environmental Engineering, University of California, Riverside, California 92521, United States

Supporting Information

ABSTRACT: Enzymes are an important class of biological molecules whose specific functionalities can be exploited to perform tasks beyond the reach of conventional chemistry. Because they are operational under environmentally friendly, ambient conditions, the adaptation of these biomacromolecules can potentially be used to replace current energy-intensive and environmentally harsh synthesis methods for materials. Here we used a hydrolytic enzyme, urease, to modify the solution environment around a water-soluble and stable TiO_2 precursor to synthesize nanocrystalline titanium dioxide under environmentally benign conditions. This urease-mediated synthesis yields nearly monodisperse TiO_2 nanostructures with high surface area that can be utilized for numerous energy-based applications such as low-cost photovoltaics and photocatalysts.

Nanocrystalline TiO_2 exhibits optoelectronic properties that are attractive for a wide range of applications such as hydrogen storage,[1] gas sensing,[2] heterogeneous photocatalysis,[3] and electrodes in dye-sensitized solar cells.[4] TiO_2 is an ideal material for these applications because of its chemical and physical stability in aqueous media, natural abundance, and minimal impact on the environment. Although TiO_2 occurs naturally as three polymorphs (brookite, rutile, and anatase), nanoscale crystalline TiO_2 often requires extensive processing at elevated temperatures and/or in many instances the use of caustic or environmentally unfriendly solvents. Vapor-phase methods for the synthesis of TiO_2 such as chemical[5] and physical vapor deposition[6] and flame pyrolysis[7] are energy-intensive and commonly result in the production of large, low-surface-area crystals. Lower-temperature solution-based routes such as hydrothermal,[8] solvothermal,[9] and sol−gel[10] methods have also been proven to be effective for the synthesis of metal oxide nanostructures but generally offer little control over the size distribution of the resulting materials.

Biomediated approaches offer pathways to the production of large-surface-area nanocrystalline materials under benign conditions such as room temperature, near-neutral pH, and in aqueous media.[11] At the heart of these biomediated approaches are biomacromolecules that are utilized either as biological constructs that template the formation of a material or as complex catalysts (i.e., enzymes) that drive a chemical reaction. Unlike traditional beaker and benchtop reactions, which use exogenous sources of reagents that often yield heterogeneities in the products resulting from their uneven distribution in solution,[12] enzymes provide precise control of a reaction by genetically derived active sites. These active sites are critical in the biological world, as their precise coordination at the angstrom level provides a low-energy pathway to complete a reaction. Biomacromolecules have been used in the past to synthesize metal oxides, including ZnO,[13] Cu_2O,[14] and Ga_2O_3.[15] Several biomacromolecular pathways for production of TiO_2 under physiological conditions have been explored. For instance, Sumerel et al.[16] demonstrated the templated synthesis of amorphous TiO_2 using the enzyme silicatein to catalyze the hydrolysis and subsequent polycondensation of the water-stable organic titanium precursor, titanium(IV) bis(ammonium lactate)dihydroxide (TiBALDH). Kroger et al.[17] produced hollow microspheres (20−50 μM in diameter) consisting of crystalline rutile TiO_2 at ambient temperature and neutral pH using the sillafin rSilC, while Luckarift et al.[18] synthesized amorphous titania at room temperature using lysozymes. Although the aforementioned methods generally employ direct templating or catalysis of the synthesized materials, similar biomediated reactions may also be used for accurate generation of the reagents, thus providing a controlled synthesis environment.

Rapid hydrolysis and condensation of precursors generally results in the formation of either amorphous or metastable structures,[19a,b] whereas controlled, uniform evolution of embryonic nuclei can result in a homogeneous size distribution among the synthesized nanomaterials.[20] Slow, uniform vapor diffusion of ammonia into a reaction medium[21,22] has generated metal oxide materials at room temperature through controlled condensation of hydrolyzed precursors, but with less control over size distribution. The uniform thermal decomposition of formamide[23] and that of urea at moderate temperatures[24] have yielded a homogeneous evolution of the solution pH to synthesize nanomaterials. The decomposition of urea, which occurs at temperatures in excess of 90 °C, results in the liberation of ammonia molecules that react with water to form ammonium hydroxide, which subsequently dissociates to form hydroxide ions and leads to a net increase in the solution pH.[25]

Conversely, the decomposition of urea can also be achieved via enzymatic routes. In aqueous solutions, urease catalyzes the decomposition of urea. The catalyzed reaction occurs 10^{14} times faster than the thermally driven hydrolysis of urea, under ambient conditions.[26] Ureases such as those present in the cell wall of the bacteria *Helicobacter pylori*, the main cause of gastritis and peptic ulceration, are used to decompose urea present in the highly

Received: July 18, 2012
Published: August 15, 2012

   dx.doi.org/10.1021/ja306884e | J. Am. Chem. Soc. 2012, 134, 13974−13977

acidic environment of the stomach in order to provide a suitable environment (i.e., neutral pH) for reproduction of the cell.[27] In plant species, urease is used to augment the intake of nitrogen that may not be available from fixation for the nitrogen cycle. A commonly investigated urease is found in the jack bean plant (*Canavalia ensiformis*). Jack bean urease (JBU), the first recognized nickel-dependent metalloenzyme,[28] consists of a hexameric structure (MW = 480 kDa) and a catalytic site consisting of Ni ions that are precisely juxtapositioned to enable the hydrolysis of urea, yielding ammonia byproducts (Figure 1a).[29] Applying this catalytic functionality, we demonstrated herein the synthesis of nanocrystalline TiO_2 at room temperature and near-neutral pH.

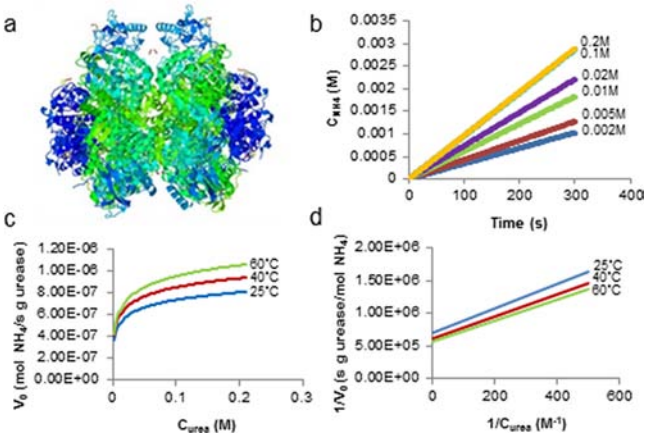

Figure 1. (a) Molecular structure of *C. ensiformis* (jack bean) urease. (b) Plots of ammonium ion concentration vs time for several different urea concentrations at room temperature. (c) Michaelis–Menten plots at 25, 40, and 60 °C. (d) Lineweaver–Burk plots at 25, 40, and 60 °C.

To determine the rate of ammonium ion production from urease under TiO_2 synthesis conditions at different temperatures (i.e., 25, 40, and 60 °C), 0.01 M solutions of TiBALDH (50 wt % in water) were prepared in nanopure water (Milli-Q) containing various concentrations of urea (i.e., 0.002, 0.005, 0.01, 0.02, 0.1, and 0.2 M) and equilibrated at the reaction temperature in a water bath. To initiate the reaction, a 1 mL suspension of JBU (0.013 μM) was injected into the TiBALDH/urea solution. Following initiation, an ammonium ion probe (Vernier) was used to monitor the ammonium ion concentration every 5 s for 5 min using Vernier LabPro software. The initial rate data were used for subsequent Michaelis–Menten and Lineweaver–Burk analyses to determine the Michaelis constant and the maximum rate of ammonium ion production, respectively, at each synthesis temperature.

Figure 1b shows the production of ammonia as a function of time at room temperature for various urea concentrations. The plots show that for urea concentrations less than 0.1 M, the rate of ammonium ion production increased with increasing urea concentration. For urea concentrations greater than 0.1 M, the rate of ammonium production was constant, implying that all of the active sites were being utilized. Similar trends were observed at 40 and 60 °C (data not shown). The corresponding Michaelis–Menten curves (Figure 1c) show that the activity of the enzyme increased with increasing temperature. The Michaelis constant K_M and the maximum reaction rate V_{max} were obtained by Lineweaver–Burk analysis of the Michaelis–Menten curves (Figure 1d). The calculated K_M values were found to be 2.70, 2.90, and 2.94 mM for the samples incubated at 25, 40, and 60 °C, respectively. The corresponding calculated V_{max} values were 1.44×10^{-6}, 1.66×10^{-6}, and 1.79×10^{-6} mol of NH_4^+ s^{-1} (mmol of enzyme)$^{-1}$. Previous studies of the activity of JBU at various temperatures have shown trends similar to those measured in the present experiments, with the urease activity increasing with increasing temperature.[30,31] It is well-known that most enzyme-catalyzed reactions initially follow an Arrhenius-based rate dependence, in which the reaction rate increases linearly with increasing temperature as a result of an increase in the probability that a substrate molecule will collide with an active site on the enzyme. The Arrhenius rate dependence continues until the onset of thermal denaturing of the enzyme, which changes its molecular conformation and deactivates sites.

To investigate the effects of reaction temperature and time on the TiO_2 crystallite size and dispersity, reactions were performed at 25, 40, and 60 °C for 12, 24, and 36 h. Briefly, an aqueous solution containing 0.1 M TiBALDH and 0.33 M urea was heated in a temperature-controlled water bath. After the desired reaction temperature was reached, a 1 mL, freshly prepared, 3.9 μM aqueous urease suspension (total urease reaction concentration = 0.13 μM) was injected into the reactor. Reactions were performed in capped glass vials under magnetic stirring at 700 rpm. The addition of urease to the mixture of the Ti precursor and urea (initial pH 7.8) initiated the formation of ammonium ions, subsequently resulting in an increase in pH. After ~2 h, the clear solution turned translucent, indicating the formation of particulate species. The reaction was allowed to continue for the desired time (i.e., 12, 24, or 36 h), with the reaction pH leveling at 9.14 after 12 h. After the reaction was stopped, the products were washed five times in nanopure H_2O, dried, and characterized using X-ray diffraction (XRD) and transmission electron microscopy (TEM).

XRD analysis of the as-synthesized materials (Figure 2a,b) uncovered reflections at 2θ = 25.3, 37.8, 48.1, and 53.9°, corresponding to the (101), (004), (200), and (105) planes, respectively, of anatase TiO_2 (JCPDS no. 01-084-1286). Scherrer analyses of the (200) reflections[32] were used to calculate the crystal diameters of TiO_2 synthesized at 25 °C for 12, 24, and 36

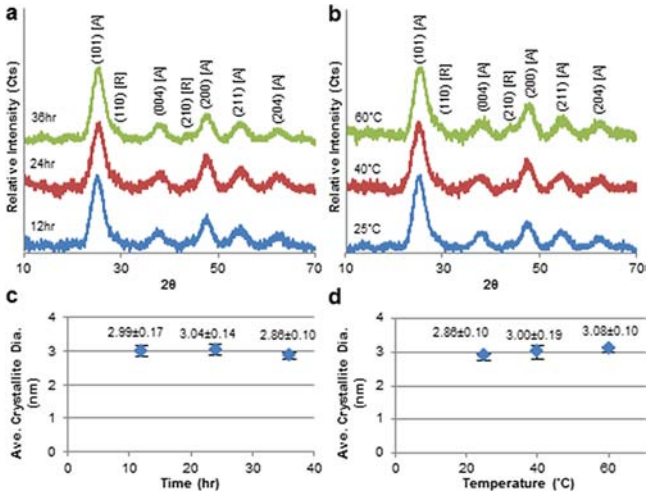

Figure 2. (a, b) XRD patterns of TiO_2 obtained by urease-mediated synthesis (a) at 25 °C for 12, 24, and 36 h and (b) at 25, 40, and 60 °C for 36 h. (c, d) Average crystallite diameters of TiO_2 nanocrystals synthesized (c) at 25 °C for 12, 24, and 36 and (d) at 25, 40, and 60 °C for 36 h.

dx.doi.org/10.1021/ja306884e | J. Am. Chem. Soc. 2012, 134, 13974–13977

h (Figure 2c) and at 40 and 60 °C for 36 h (Figure 2d). It is clear that the average TiO_2 crystallite size remained nearly constant at ~3.0 nm under these reaction conditions. In addition to the anatase reflections, two minor peaks observed at 27.4 and 44.0° may indicate the presence of rutile TiO_2 (JCDPDS no. 01-073-1765). However, further evaluation is necessary to confirm this.

To confirm the size and phase of the as-synthesized materials, samples were imaged using bright-field TEM imaging and selected-area electron diffraction (SAED). High-resolution bright-field TEM images of the samples prepared at 25, 40, and 60 °C for 36 h (Figure 3a–c, respectively) all demonstrate

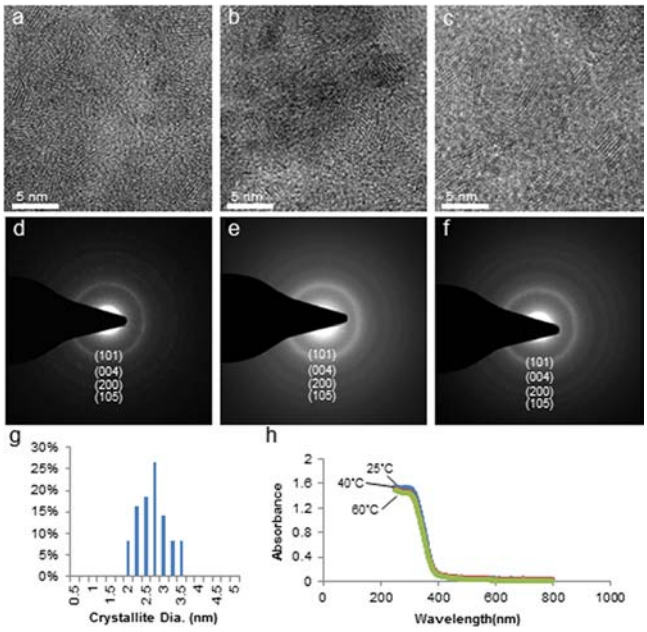

Figure 3. (a–c) Bright-field TEM images of urease-mediated TiO_2 prepared at (a) 25, (b) 40, and (c) 60 °C for 36 h and (d–f) corresponding SAED patterns, which reveal a nanocrystalline anatase structure. (g) Representative histogram of the crystallite size distribution for the material synthesized at 25 °C for 36. (h) UV–vis spectra of TiO_2 synthesized at 25, 40, and 60 °C for 36 h.

similar crystallite diameters (~3 nm). Lattice imaging also confirmed anatase TiO_2, with nanocrystal *d* spacings of 3.51 ± 0.2 Å [i.e., (101) anatase]. The SAED patterns of the specimens (Figure 3d–f) showed the presence of nanocrystalline anatase TiO_2, confirming the XRD observations.

It was anticipated that a metastable phase such as anatase would form because the energy landscape seen by the reaction, which occurs at low temperature, should often pass through metastable phases on its way to the final crystalline state (i.e., rutile). These pathways often have lower energy barriers, as is the case for nucleation of anatase versus rutile.[33] In fact, many methods for the synthesis of TiO_2 often form anatase first.[34,35] Structurally, the long-range arrangement of the TiO_6 octahedra in anatase is less constrained than in rutile.[36] In addition, anatase has a lower surface free energy, even though rutile has a lower Gibbs free energy,[37] and thus, anatase may be the more favored crystalline phase because of the high surface energy of rutile crystallites.[33]

The nanocrystal sizes and size distribution of each specimen were determined by measuring at least 50 nanocrystals per sample from TEM micrographs similar to those in Figure 3a–c. A representative histogram for the sample prepared at 25 °C for 36 h is shown in Figure 3g. Similar histograms were observed for samples prepared at 40 and 60 °C (data not shown). It is clear that the samples had a narrow size distribution (e.g., 2.8 ±0.34 nm for the sample prepared at 25 °C for 36 h), indicating coordinated hydrolysis and condensation of the precursor leading to controlled nucleation and growth of the TiO_2 nanocrystals. In comparison, anatase TiO_2 prepared without enzyme (i.e., by adding exogenous base) under similar pH, temperature and time conditions displayed smaller average crystallite domains (2.28 nm ±0.80) but a larger distribution (Figure 1 in the Supporting Information), highlighting the uniformity of the enzyme-mediated process. These coordinated reactions are related to the hydrolytic stability of TiBALDH due to the interaction of adjacent oxygen and carboxylate functional groups with the metal center. This conjugate system allows for delocalization of electrons away from the oxygen molecule complexed to the central metal ion, which reduces the Lewis basicity of the coordinated oxygen atom.[38] Thus, the homogeneous dispersion of urease throughout the solution coincides with a homogeneous increase in the OH^- concentration, which enables simultaneous nucleophilic attack of free OH^- ions on the juxtaposed bidentate ligands coordinatively attached to the central Ti^{4+} ion.[8] These nucleophilic ions hydrolyze the TiBALDH, leading to the formation of fully (and partially) hydrolyzed species that can participate in condensation reactions. This is advantageous in comparison with the addition of an exogenous base, which reacts with TiBALDH molecules located at the surface of the reaction medium before those that are at the bottom of the reactor.

The increase in pH from the initial pH of ~7.8 to the synthesis pH of ~8.65 over a 1 h period represents nearly an order of magnitude increase in the OH^- concentration. This uniform generation of hydroxide ions in the reaction solution ensures that a significant fraction of the TiBALDH molecules hydrolyzes at the same rate. If the speciation of $Ti(BALDH)_{2-n}(OH)_{2+n}$ is nearly the same, then the rate of growth of condensed species will also be similar, and thus, the induction time to nucleation (i.e., the time from the when the solution acquires a state of supersaturation to the formation of nuclei of critical size[39]) will be uniform. The induction time is related to the nucleation rate[40] and is strongly dependent on the supersaturation. Thus, by controlling the concentration of (i) enzyme, (ii) urea, and (iii) TiBALDH, we can control the hydrolysis of TiBALDH to form Ti–OH species, which subsequently condense to form Ti–O–Ti clusters; therefore, controlling the supersaturation makes the nucleation rate uniform throughout the solution.

The crystallite diameters of the synthesized TiO_2 were approximately constant regardless of reaction duration or solution temperature, indicating that significant growth was hindered. It has been shown that lactic acid has an affinity for TiO_2 surfaces,[41] and thus, the hydrolyzed lactato ligand byproduct likely adsorbed to the surface of the newly formed nanocrystals, hindering diffusion of growth units onto the crystallite surface. Mockel et al.[42] demonstrated this phenomenon by injecting ammonium lactate into a hydrothermal reactor at the onset of a reaction using TiBALDH as a precursor to form TiO_2. The result was a 50% reduction in the size of the TiO_2 crystallites versus those prepared without extraneous lactate groups. The reactions in this study were performed at significantly lower temperatures than under hydrothermal conditions, and it is therefore also feasible that the growth could be limited by not only lactate absorption but also sluggish growth kinetics.

dx.doi.org/10.1021/ja306884e | J. Am. Chem. Soc. 2012, 134, 13974–13977

UV−vis spectra (Figure 3h) were also obtained for TiO_2 synthesized at 25, 40, and 60 °C for 36 h. The band gaps measured from these spectra were determined to be 3.22, 3.21, and 3.19 eV, respectively. Although there is a slight decrease in the observed band gap with increasing synthesis temperature, the results are within the margin of error and are therefore considered constant. The measured band gaps are also similar to those observed in previous investigations[43−45] and reflect the predicted band gap for anatase TiO_2.

We have demonstrated a biomediated approach in which the hydrolytic enzyme urease is used to induce a uniform dispersion of anatase TiO_2 at room temperature. This is achieved through coordination of the enzyme with urea in a solution containing a hydrolytically stable TiO_2 precursor. The lag time between injection of urease and generation of hydroxide ions in solution affords coordinated hydrolysis and condensation of the precursor molecules, resulting in a single-burst nucleation event. In addition, the use of an enzyme to generate the reagent (i.e., hydroxide ions) circumvents the need for thermal decomposition of formamide or urea, and thus, the reaction can be sustained at room temperature, which enables the growth of these materials on polymeric substrates (e.g., electrically conductive polymers as electrodes for flexible sensitized solar cells). Eventually, immobilization of these enzymes will afford opportunities to use and reuse them as room-temperature catalysts for low-cost syntheses of metal oxides.

■ ASSOCIATED CONTENT

Supporting Information

Experimental procedures and details concerning XRD and TEM characterization. This material is available free of charge via the Internet at http://pubs.acs.org.

■ AUTHOR INFORMATION

Corresponding Author

david@engr.ucr.edu

Present Address

†Lawrence Berkeley National Laboratory, Berkeley, CA 94720.

Notes

The authors declare no competing financial interest.

■ ACKNOWLEDGMENTS

We acknowledge the Central Facility for Advanced Microscopy and Microanalysis (CFAMM) at UC Riverside for assistance with TEM. Additional TEM analysis was performed as a user project at The Molecular Foundry, Lawrence Berkeley National Laboratory, which is supported by the Office of Science, Office of Basic Energy Sciences, of the U.S. Department of Energy under Contract DE-AC02-05CH11231.

■ REFERENCES

(1) Schlapbach, L.; Zuttel, A. *Nature* **2001**, *414*, 353.
(2) Ruiz, A. M.; Sakai, G.; Cornet, A.; Shimanoe, K.; Morante, J. R.; Yamazoe, N. *Sens. Actuators, B* **2003**, *93*, 509.
(3) Ashokkumar, M. *Int. J. Hydrogen Energy* **1998**, *23*, 427.
(4) O'Regan, B.; Grätzel, M. *Nature* **1991**, *353*, 737.
(5) O'Neill, S. A.; Parkin, I. P.; Clark, R. J. H.; Mills, A.; Elliot, N. *J. Mater. Chem.* **2003**, *13*, 56.
(6) Xiang, B.; Zhang, Y.; Wang, Z.; Luo, X. H.; Zhu, Y. W.; Zhang, H. Z.; Yu, D. P. *J. Phys. D: Appl. Phys.* **2005**, *38*, 1152.
(7) Khan, S. U. M.; Al-Shahry, M.; Ingler, W. B., Jr. *Science* **2002**, *297*, 2243.
(8) Kinsinger, N. M.; Wong, A.; Li, D.; Villalobos, F.; Kisailus, D. *Cryst. Growth Des.* **2010**, *10*, 5254.
(9) Wahi, R. K.; Liu, Y.; Falkner, J. C.; Colvin, V. L. *J. Colloid Interface Sci.* **2006**, *302*, 530.
(10) Livage, J.; Sanchez, C.; Henry, M.; Doeuff, S. *Solid State Ionics* **1989**, *32/33*, 633.
(11) Shimizu, K.; Cha, J.; Stucky, G. D.; Morse, D. E. *Proc. Natl. Acad. Sci. U.S.A.* **1998**, *95*, 6234.
(12) Matijevic, E. *Chem. Mater.* **1993**, *5*, 412.
(13) Umetsu, M.; Mizuta, M.; Tsumoto, K.; Ohara, S.; Takami, S.; Watanabe, H.; Kumagai, I.; Adschiri, T. *Adv. Mater.* **2005**, *17*, 2571.
(14) Thai, C. K.; Dai, H.; Sastry, M. S. R.; Sarikaya, M.; Schwartz, D. T.; Baneyx, F. *Biotechnol. Bioeng.* **2004**, *87*, 130.
(15) Kisailus, D.; Choi, J. H.; Weaver, J. C.; Yang, W.; Morse, D. E. *Adv. Mater.* **2005**, *17*, 314.
(16) Sumerel, J. L.; Yang, W.; Kisailus, D.; Weaver, J. C.; Choi, J. H.; Morse, D. E. *Chem. Mater.* **2003**, *15*, 4804.
(17) Kroger, N.; Dickerson, M. B.; Ahmad, G.; Cai, Y.; Haluska, M. S.; Sandhage, K. H.; Poulsen, N.; Sheppard, V. C. *Angew. Chem., Int. Ed.* **2006**, *45*, 7239.
(18) Luckarift, H. R.; Dickerson, M. B.; Sandhage, K. H.; Spain, J. C. *Small* **2006**, *5*, 640.
(19) (a) Sun, C.; Xue, D. *Curr. Opin. Chem. Eng.* **2012**, *1*, 108. (b) Sun, C.; Xue, D. *Rev. Adv. Sci. Eng.* **2012**, *1*, 4.
(20) Adachi-Pagano, M.; Forano, C.; Besse, J. *J. Mater. Chem.* **2003**, *13*, 1988.
(21) Kisailus, D.; Schwenzer, B.; Gomm, J.; Weaver, J. C.; Morse, D. E. *J. Am. Chem. Soc.* **2006**, *128*, 10276.
(22) Schwenzer, B.; Roth, K. M.; Gomm, J. R.; Murr, M.; Morse, D. E. *J. Mater. Chem.* **2006**, *16*, 401.
(23) Kometani, N.; Fujita, A.; Yonezawa, Y. *J. Mater. Sci.* **2008**, *43*, 2942.
(24) Yang, R.; Yu, H.; Li, M. *J. Mater. Sci. Lett.* **2003**, *22*, 1131.
(25) Cesareo, S. D.; Langton, S. R. *FEMS Microbiol. Lett.* **1992**, *99*, 15.
(26) Lippard, S. J. *Science* **1995**, *268*, 996.
(27) Mobley, H. L. T.; Island, M. D.; Hausinger, R. P. *Microbiol. Rev.* **1995**, *59*, 451.
(28) Dixon, N. E.; Gazzola, C.; Blakeley, R. L.; Zerner, B. *J. Am. Chem. Soc.* **1975**, *97*, 4131.
(29) Balasubramanian, A.; Ponnuraj, K. *J. Mol. Biol.* **2010**, *400*, 274.
(30) Lai, C. M.; Tabatabai, M. A. *Soil Biol. Biochem.* **1992**, *24*, 225.
(31) Cevik, E.; Senel, M.; Abasiyank, M. F. *Afr. J. Biotechnol.* **2011**, *10*, 6590.
(32) Murakami, N.; Kurlhara, Y.; Tsubota, T.; Ohno, T. *J. Phys. Chem. C* **2009**, *113*, 3062.
(33) Hanaor, D. A. H.; Sorrell, C. C. *J. Mater. Sci.* **2011**, *46*, 855.
(34) Okada, K.; Yamamoto, N.; Kameshima, T.; Yasumori, A. *J. Am. Ceram. Soc.* **2001**, *84*, 1591.
(35) Shin, H.; Jung, H. S.; Hong, K. S.; Lee, J.-K. *J. Solid State Chem.* **2005**, *178*, 15.
(36) Matthews, A. *Am. Mineral.* **1976**, *61*, 419.
(37) Zhang, H. Z.; Banfield, J. F. *J. Mater. Chem.* **1998**, *8*, 2073.
(38) Casey, W. H.; Phillips, B. L.; Nordin, J. P.; Sullivan, D. J. *Geochim. Cosmochim. Acta* **1998**, *62*, 2789.
(39) Garcia-Ruiz, J. M. *J. Struct. Biol.* **2003**, *142*, 22.
(40) De Yoreo, J. J.; Vekilov, P. G. *Rev. Mineral. Geochem.* **2003**, *54*, 57.
(41) Awatani, T.; Dobson, K. D.; McQuillan, A. J.; Ohtani, B.; Uosaki, K. *Chem. Lett.* **1998**, 849.
(42) Mockel, H.; Giersig, M.; Willig, F. *J. Mater. Chem.* **1999**, *9*, 3051.
(43) Reddy, K. M.; Manorama, S. V.; Reddy, A. R. *Mater. Chem. Phys.* **2003**, *78*, 239.
(44) Knorr, F. J.; Zhang, D.; McHale, J. L. *Langmuir* **2007**, *23*, 8686.
(45) McHale, J. L. Knorr, F. Photoluminescence and Carrier Transport in Nanocrystalline TiO_2. In *Handbook of Luminescent Semiconductor Materials*; Bergman, L., McHale, J. L., Eds.; CRC Press: Boca Raton, FL, 2011; pp 365−390.